Supporting Information

Li et al. 10.1073/pnas.1216499110

SI Methods

Synthesis of CDE-096. The synthesis of CDE-096 is outlined in Scheme 1. Unless otherwise specified, all reactions were performed in oven-dried glassware with magnetic stirring under an atmosphere of dry nitrogen. Tetrahydrofuran (THF) was purified by distillation over sodium benzophenone ketyl. All commercially obtained reagents and solvents were used without further purification. 3,4,5-Tribenzylgallate was prepared by the procedure described previously (1).

Analytical TLC was performed on silica gel–coated glass plates (Sorbent Technologies; 250 μm silica gel with UV254) and visualized with UV light. Flash column chromatography was performed using silica gel (Sorbent Technologies Premium Rf; 60 Å, 40–75 μM) and used the indicated solvent.

All ^{1}H NMR spectra were recorded on a Jeol ECX-400 (400 MHz) spectrometer. ^{13}C NMR spectra were recorded on a Jeol ECX-400 (100 MHz) spectrometer. The proton signal of residual, nondeuterated solvent (δ 7.26 for $CHCl_3$, δ 2.50 for DMSO, δ 2.05 for acetone) was used as an internal reference for ^{1}H spectra, whereas the chemical shifts for ^{13}C spectra are reported relative to the δ 77.0 resonance for $CDCl_3$, δ 39.5 resonance for DMSO, and the δ 206.3 resonance for acetone. Coupling constants (J) are expressed in Hertz. Splitting patterns are indicated as follows: s (singlet), bs (broad singlet) d (doublet), t (triplet), q (quartet), quin (quintet), dd (doublet of doublets), and m (multiplet). Electrospray (ES) high-resolution mass spectra were recorded on a VG 70–250-s spectrometer manufactured by Micromass Corp. at the University of Michigan Mass Spectrometry Laboratory.

tert-Butyl *N*-(2,3-dihydroxypropyl)carbamate (1.00 g, 5.23 mmol), 3,4,5-tribenzylgallate (5.77 g, 13.1 mmol), 4-dimethylaminopyridine (DMAP, 0.16 g, 1.31 mmol), and CH_2Cl_2 (5.00 mL) were combined and stirred under N_2. In a separate flask, 1-ethyl-3-(3-dimethylaminopropyl)carbodiimide hydrochloride (EDC·HCl, 2.70 g, 13.1 mmol) and CH_2Cl_2 (10 mL) were mixed at 0 °C and then syringed into the reaction flask in a dropwise manner. The reaction stirred at room temperature overnight under N_2. The organic layer was washed with 1 N HCl (2×), saturated aqueous sodium bicarbonate (2×), and brine (1×), dried over $MgSO_4$, filtered, and concentrated in vacuo. The residue was purified by column chromatography (all concentrations are given as vol/vol) (60% hexanes/ethyl acetate) to obtain diester **1** as a white solid (4.12 g, 76%). ^{1}H NMR ($CDCl_3$, 400 MHz) δ 7.36–7.24 (m, 34H), 5.42 (quin, J = 4.6 Hz, 1H), 5.06 (m, 12H), 4.82 (t, J = 5.95 Hz), 4.59 (dd, J = 11.9, 4.1 Hz, 1H), 4.46 (dd, J = 11.9, 6.4 Hz, 1H), 3.54 (m, 2H), and 1.44 (s, 9H); ^{13}C NMR ($CDCl_3$, 100 MHz) δ 165.82, 165.63, 155.91, 152.64, 142.89, 142.70, 137.48, 137.43, 136.62, 128.62, 128.58, 128.30, 128.28, 128.16, 128.13, 128.08, 128.04, 127.67, 124.65, 109.44, 109.19, 79.99, 75.19, 71.93, 71.33, 71.21, 63.53, 60.52, 41.12, 28.45.

Diester **1** (0.150 g, 0.15 mmol) and CH_2Cl_2 (0.50 mL) were combined and held at 0 °C under N_2. Trifluoroacetic acid (0.50 mL, 6.73 mmol) was syringed dropwise into the flask with stirring. After 10 min, TLC (50% hexanes/ethyl acetate) indicated the consumption of starting material. The solvent was evaporated in vacuo, and ethyl acetate (5.00 mL) was added and evaporated three times successively to remove excess trifluoroacetic acid and provide the deprotected trifluoroacetic acid (TFA) salt as a white solid (97.9 mg, 72%), which was used without further purification. The crude TFA salt (0.20 g, 0.19 mmol), pyridine (0.50 mL), and 3-(trifluoromethyl)phenyl chloroformate (0.36 μL, 0.23 mmol) were combined and stirred at room temperature for 24 h. The reaction was diluted with ethyl acetate, and the organic layer was washed with 1 N HCl (2×), saturated aqueous sodium bicarbonate (2×), and brine (1×), dried over $MgSO_4$, filtered, and concentrated in vacuo. The residue was purified by column chromatography (50% hexanes/ethyl acetate) to give aryl carbamate **2** as a tan solid (135 mg, 63%). ^{1}H NMR ($CDCl_3$, 400 MHz) δ 7.36–7.25 (m, 38H), 5.47 (m, 1H), 5.05 (m, 12H), 4.65 (dd, J = 11.9, 5.0 Hz, 1H), 4.51 (dd, J = 11.9, 6.0 Hz, 1H), 3.75 (m, 1H), 3.63 (m, 1H).

Aryl carbamate **2** (0.134 g, 0.12 mmol), THF (2.00 mL), and 10% Pd°/C (0.13 g, 1.19 mmol) were combined and stirred for 36 h at 40 °C under a balloon of H_2. The reaction mixture was syringed through a polytetrafluoroethylene 0.2-μM syringe filter to remove the Pd/C catalyst. The solvent was then removed in vacuo and triturated with hexanes to obtain CDE-096 as a buff solid (59.1 mg, 85%) with >95% purity by NMR. ^{1}H NMR (acetone-d_6, 400 MHz) δ 7.55 (m, 2H), 7.45 (bs, 1H), 7.37 (m, 2H), 7.14 (s, 2H), 7.11 (s, 2H), 5.50 (m, 1H), 4.55 (dd, J = 12 Hz, 4 Hz, 1H), 4.48 (dd, J = 12 Hz, 5 Hz, 1H), 3.69 (m, 2H); ^{13}C NMR (acetone-d_6, 100 MHz) δ 165.69, 165.56, 154.43, 151.87, 145.15, 145.10, 138.08, 138.05, 130.98 (q, J = 32 Hz), 130.33, 127.77, 125.83, 124.01 (q, J = 270 Hz), 121.72, 121.69, 120.70, 120.59, 118.76, 118.73, 109.34, 109.15, 70.74, 63.28, 41.57.; high-resolution mass spectrometry, ES calculated for $C_{25}H_{20}F_3NO_{12}Na$ $[M+Na]^+$ 606.0835, found: 606.0821.

X-Ray Crystallography. Before crystallization, native plasminogen activator inhibitor type-1 $(PAI\text{-}1)_{14–1b}$ in 50 mM sodium phosphate, 100 mM NaCl, and 1 mM EDTA, pH 6.6, was buffer exchanged into 25 mM Tris, pH 7.5, and 250 mM NaCl, and concentrated to 2.9 mg/mL. Drops containing 2 μL of protein mixed with 2 μL of well solution were set up in vapor diffusion experiments at room temperature against 0.99–1.54 M ammonium sulfate, 200 mM NaCl, and 100 mM Na cacodylate, pH 6.5–6.8. Native crystals were soaked for 24 h in well solution containing 0.5 mM CDE-096 and then back-soaked briefly in cryoprotective solution containing well solution with 25% ethylene glycol. Crystals diffracted to 2.19-Å resolution at the Advanced Photon Source LS-CAT 21-ID-D beamline, and the diffraction data were processed with HKL2000 (2) into space group C2 with a unit cell of a = 134.96 Å, b = 65.50 Å, c = 96.99 Å; α = 90°, β = 100.619, γ = 90°.

The structure was solved with two molecules in the asymmetric unit via molecular replacement methods using Phaser (3) and a previous in-house native structure of PAI-1 as the search model. The structure went through iterative rounds of electron density map fitting in Coot (4) and structural refinement in Buster (5). Residues 6–331, 349–379 for monomer A and 4–331, 340–379 for monomer B were visible in the 2Fo-Fc electron density maps. Difference electron density maps contoured to 3s showed the presence of two CDE-096 molecules (Fig. S6 *B* and *C*). 3D coordinates and restraint files for CDE-096 were created by Grade using the mogul+qm option in Buster (5). The CDE-096 coordinates were fit into electron and refined. Statistics for the refined structure are given in Table S1. The structure was validated using Whatcheck (6), Molprobity (7), and Pavarti (8). The refined structure had 98.61% of its residues in the favored regions of a ramanchandran plot, a molprobity score of 1.22, and a clashscore of 4.43.

For the cocrystal structure, $PAI\text{-}1_{14–1b}$ was buffer exchanged into 25 mM Tris, pH 7.5, and 250 mM NaCl and then incubated in a 1:1.5 ratio with CDE-096 at room temperature for 1 h. The protein-inhibitor complex was then concentrated to 2.9 mg/mL

and set up in crystallization trays under the same conditions as the native protein. The crystals diffracted to 2.75 Å at LS-CAT 21-ID-D beamline and was processed into P1 space group having unit cell $a = 65.33$ Å, $b = 75.317$ Å, $c = 105.002$, Å; $\alpha = 91.32°$, $\beta = 93.49°$, $\gamma = 115.65°$ and four molecules in the asymmetric unit.

The structure was solved, refined, and validated in the same manner as the soaked crystal structure. Residues 5–331, 349–379 were apparent in electron density for monomers A and B. Residues 5–331, 341–379 were represented by electron density for monomers C and D. Difference electron density maps showed the presence of a blob and trail of waters that was modeled as a partially occupied CDE-096 molecule (Fig. S6*A*). The structure was validated using Whatcheck (6), Molprobity (7), and Pavarti (8). The refined structure had 97.56% of its residues in the favored regions of a ramanchandran plot, a molprobity score of 1.73, and a clashscore of 4.85.

Data collection and refinement statistics are shown in Table S1. The PAI-1/CDE-096 cocrystal and soaked forms were deposited into the Research Collaboratory for Structural Bioinformatics Protein Data Bank with PDB ID codes 4G8O and 4G8R, respectively.

1. Ren Y, Himmeldirk K, Chen X (2006) Synthesis and structure-activity relationship study of antidiabetic penta-O-galloyl-D-glucopyranose and its analogues. *J Med Chem* 49(9): 2829–2837.
2. Otwinowski Z, Minor W (1997) Processing of X-ray Diffraction Data Collected in Oscillation Mode. *Methods in Enzymology: Macromolecular Crystallography, part A*, eds Carter CW, Jr., Sweet RM (Academic Press, New York), Vol 276, pp 307–326.
3. McCoy AJ, et al. (2007) Phaser crystallographic software. *J Appl Cryst* 40(Pt 4):658–674.
4. Emsley P, Cowtan K (2004) Coot: model-building tools for molecular graphics. *Acta Crystallogr D Biol Crystallogr* 60(Pt 12 Pt 1):2126–2132.
5. Roversi P, Sharff A, Smart OS, Vonrhein C, Womack TO (2011) *BUSTER Version X.Y.Z* (Global Phasing Ltd., Cambridge,UK).
6. Hooft RWW, Vriend G, Sander C, Abola EE (1996) Errors in protein structures. *Nature* 381(6580):272.
7. Davis IW, et al. (2007) MolProbity: All-atom contacts and structure validation for proteins and nucleic acids. *Nucleic Acids Res* 35(Web Server issue):W375–W383.
8. Zucker F, Champ PC, Merritt EAV (2010) Validation of crystallographic models containing TLS or other descriptions of anisotropy. *Acta Crystallogr D Biol Crystallogr* 66(Pt 8):889–900.

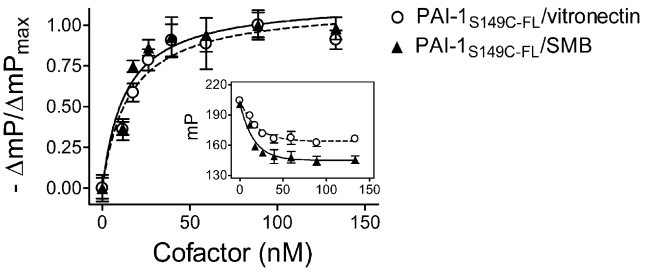

Fig. S1. Fluorescein-labeled PAI-1 allows the detection of cofactor-binding in solution via changes in florescence polarization. PAI-1$_{S149C-FL}$ at 5 nM was incubated with concentrations of vitronectin (○) or SMB (▲) for 15 min, and the fluorescence polarization (FP) was measured as described (*Inset*). The data were normalized and fit to a single-site binding equation (main axes). In agreement with previous reports, vitronectin and SMB showed virtually identical affinities for PAI-1 (apparent K_D values of 15 ± 5 and 13 ± 4 nM, respectively).

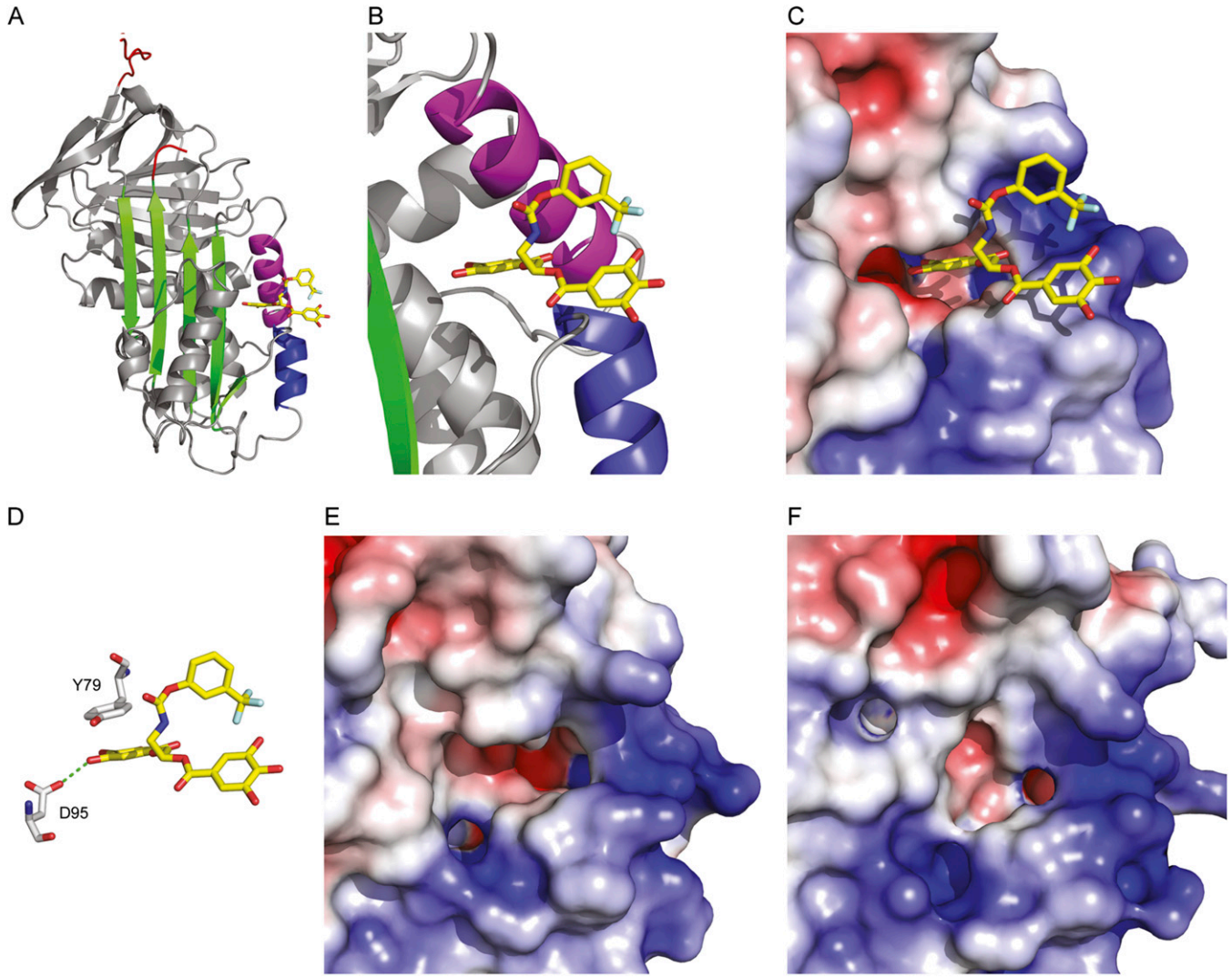

Fig. S2. A second CDE-096 binding site is observed only in the crystal soaking studies containing high concentrations of CDE-096. (*A* and *B*) Ribbon and (*C*) electrostatic surface renderings of the previously defined A β-sheet (sA)/α-helix D (hD) site (more positively charged regions in blue, and more negatively charged regions in red). A CDE-096 gallate inserts asymmetrically into a large pocket that is lined by mostly acidic residues, whereas the other gallate and the carbamate derivative project into space, with no further predicted contacts with PAI-1. (*D*) Only one hydrogen bond is predicted with Asp95, whereas potential hydrophobic interactions are more prominent, including pi-stacking between the inserted gallate and Tyr79. However, mutation of these residues did not alter the IC_{50} of inactivation by CDE-096 compared with WT PAI-1 (Fig. 5*F*). (*E* and *F*) The sA/hD pocket shows major structural changes upon transition from the (*E*) native to the (*F*) latent conformation, which are inconsistent with the observation that the binding of CDE-096 to native and latent PAI-1 is essentially identical (Fig. 4*A*). Together, the data strongly suggest the binding of CDE-096 to sA/hD pocket is a an artifact of the soaking experiment with no contribution to the formation of the high-affinity PAI-1/CDE-096 complex.

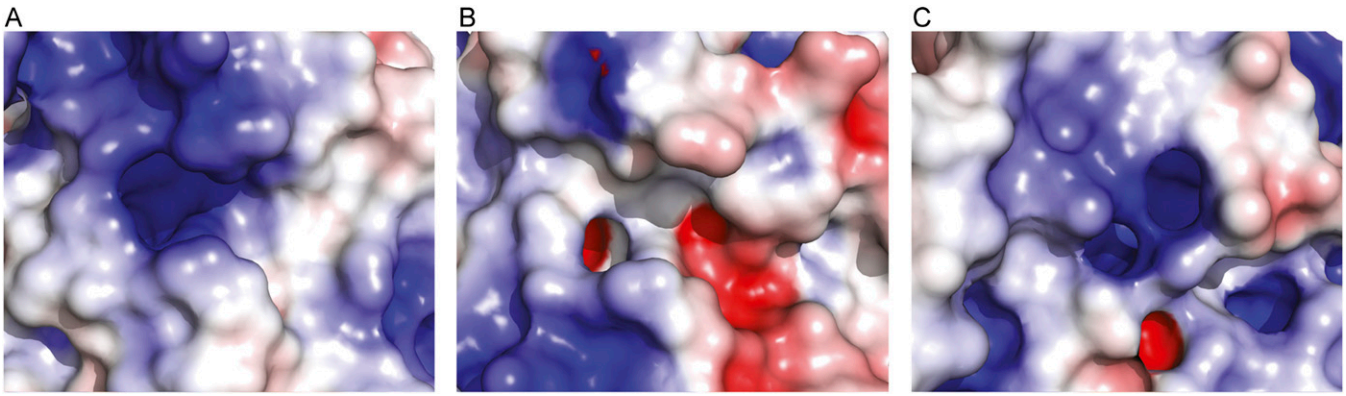

Fig. S3. The structure of the sB/sC pocket varies among closely related serpins. Electrostatic potential surface renderings of PAI-1 (*A*), antithrombin (*B*, PDB ID code 1T1F), and α_1-PI (*C*, PDB ID code 1QLP) shows that the sB/sC pockets on these closely related serpins are structurally different (more positively charged regions in blue, and more negatively charged regions in red). Chemically and structurally compatible with CDE-096, the sB/sC site in PAI-1 consists of a solvent-accessible hydrophobic pocket with a rim of basic residues. In contrast, the homologous site in antithrombin shows prominent acidic surface residues in the vicinity of a much smaller pocket. The sB/sC site in α_1-PI forms a shallow, positively charged depression. These observations provide a structural basis for the exquisite specificity of CDE-096 for PAI-1 (Table 1).

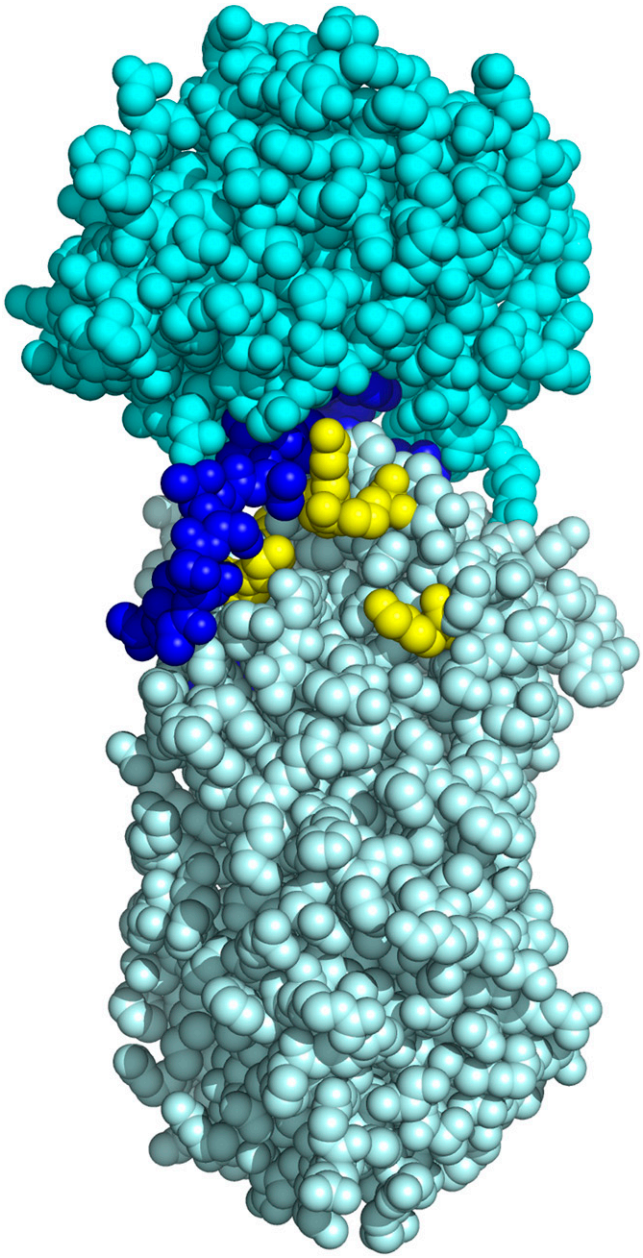

Fig. S4. CDE-096 binds to PAI-1 adjacent to the intermolecular interface of the PAI-1/uPA noncovalent complex. Residues (yellow) indicated by site-directed mutagenesis to be involved in high-affinity binding of CDE-096 are shown in the noncovalent PAI-1/uPA Michaelis complex (PDB ID code 3PB1). In the spacefill rendering shown, the CDE-096 binding site is positioned adjacent to the RCL (blue) and reveals one way by which CDE-096 could deter the binding of uPA (teal). The remainder of PAI-1 is shown in cyan. Together, the structural model and the biochemical data suggest that CDE-096 may both sterically and allosterically prevent the PAI-1 RCL from adopting an optimal conformation for protease binding.

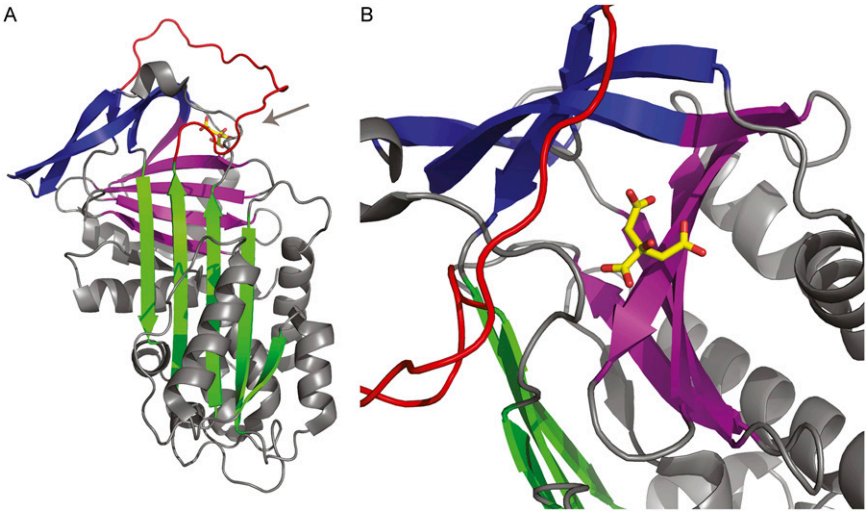

Fig. S5. Citrate binds to the sB/sC pocket of α_1-PI. The sB/sC pocket is functionally significant in another serpin of clinical importance. A naturally occurring α_1-PI variant is known to cause cirrhosis and emphysema through misfolding, aggregation, and generation of proinflammatory inclusion bodies in the liver. These proinflammatory inclusions lead to liver damage, and α_1-PI deficiency results in the dysregulation of serine proteases, like elastase, which damage connective tissue at crucial sites such as the in the lung. In vitro, citrate has been shown to prevent misfolding of native α_1-PI by binding to the sB/sC pocket (arrow in *A*). Shown are (*A*) wide and (*B*) detailed views of the X-ray crystal structure of the α_1-PI/citrate complex, where sA is in green, sB is in purple, sC is in blue, the RCL is in red, and citrate is in yellow with oxygens in red (PDB ID code 3CWM).

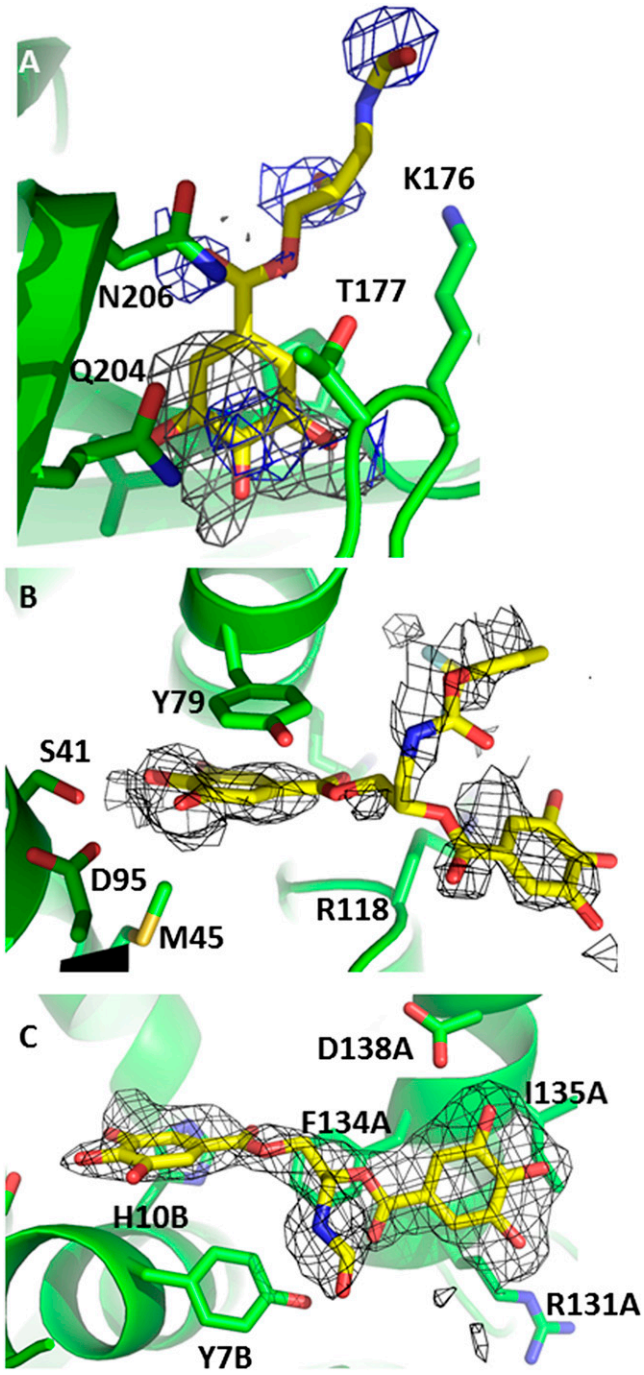

Fig. S6. Omit maps (Fo-Fc electron density) for CDE-096 binding sites in PAI-1. PAI-1 molecules are shown as green ribbons with residues interacting with CDE-096 molecules shown as ball-n-sticks (carbons in green, nitrogens in blue, and oxygens in red). CDE-096 molecules are shown as ball-n-sticks with carbons in yellow, nitrogens in blue, and oxygens in red. Difference electron density maps are shown as black grids. (*A*) High affinity binding site with omit difference electron density map contoured at 2.5 σ and the blue omit 2Fo-Fc electron density map contoured at 1 σ. (*B*) Low affinity binding site with density contoured at 2.0 σ. (*C*) Dimer interface binding site resulting from soaking native crystals in solution containing CDE-096 with density contoured at 3 σ. Residues from the *A* and *B* monomers are designated in the label after the residue number.

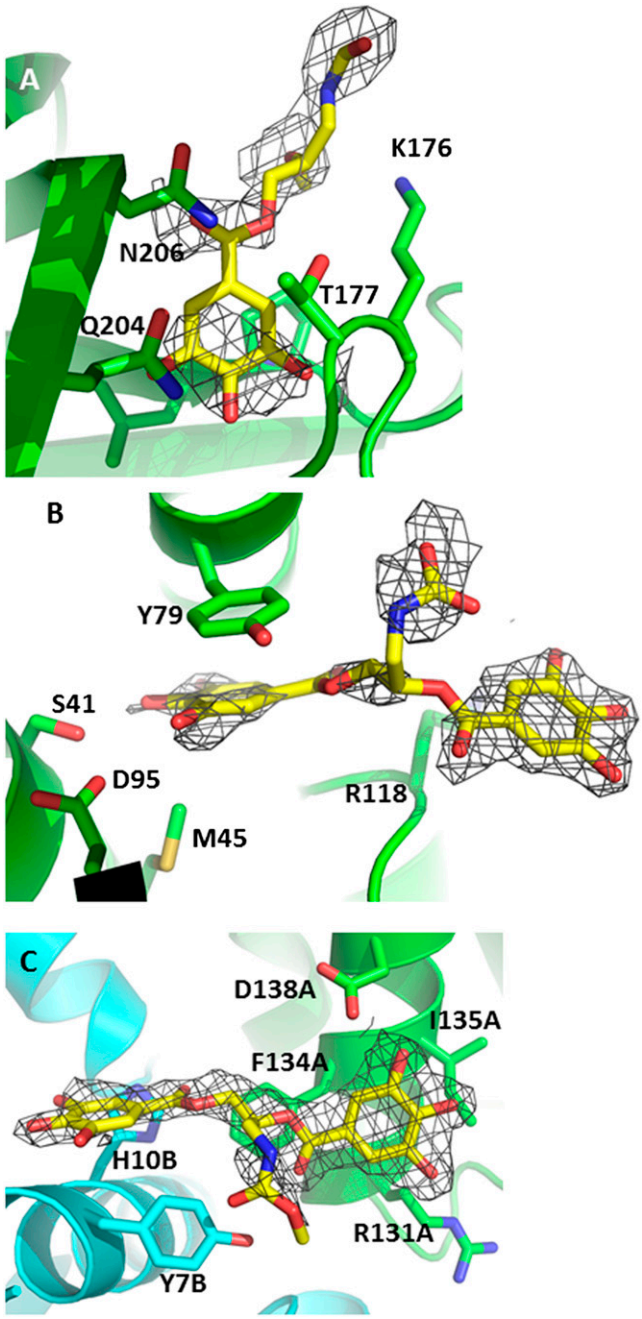

Fig. S7. The refined 2Fo-Fc electron density for CDE-096 binding sites in PAI-1. PAI-1 molecules are shown as green ribbons with residues interacting with CDE-096 molecules shown as ball-n-sticks (carbons in green, nitrogens in blue, and oxygens in red). CDE-096 molecules are shown as ball-n-sticks with carbons in yellow, nitrogens in blue, and oxygens in red. Difference electron density maps are shown as black grids. (*A*) High affinity binding site with difference electron density map contoured at 0.8 σ. (*B*) Low affinity binding site with density contoured at 1.0 σ. (*C*) Dimer interface binding site resulting from soaking native crystals in solution containing CDE-096 with density contoured at 1 σ. Residues from the *A* and *B* monomers are designated in the label after the residue number and shown in green and blue, respectively.

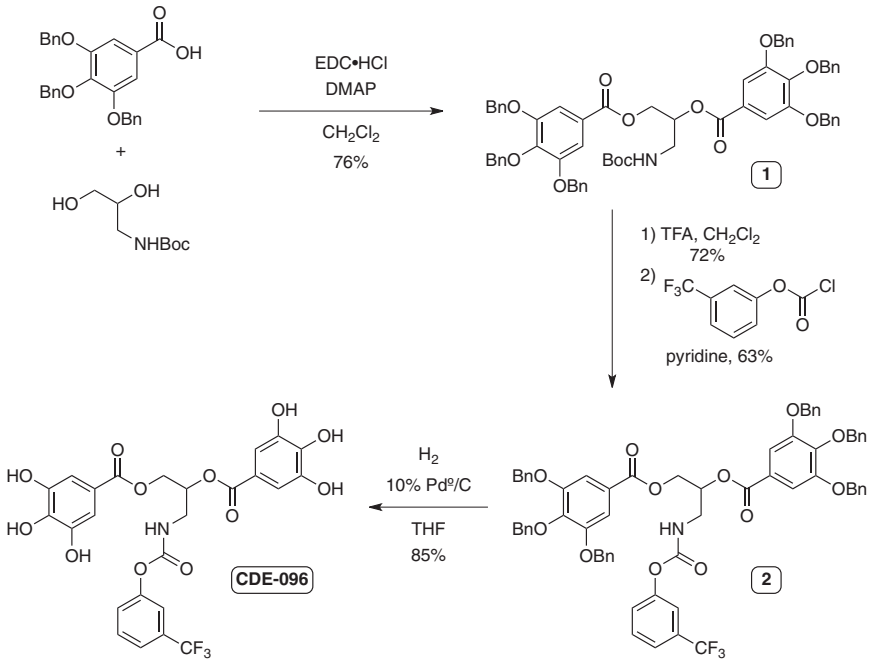

Scheme 1. The synthesis reaction for CDE-039.

Table S1. Data collection and refinement statistics (molecular replacement)

Data collection	PAI-1/CDE-096 (cocrystal)	PAI-1/CDE_096 (soak)
Space group	P1	C2
Cell dimensions		
a, b, c (Å)	65.34, 75.32, 105.00	134.96, 65.50, 96.99
α, β, γ (°)	91.32, 93.49, 115.65	90.00, 100.62, 90.00
Resolution (Å)*	2.75 (2.75–2.80)	2.19 (2.24–2.19)
R_{sym}[†]	0.085 (0.351)	0.095 (0.367)
I/σI[‡]	10 (2)	20 (3)
Completeness (%)[§]	93.4 (96.0)	99.9 (99.4)
Redundancy	2.3 (2.3)	7.2 (6.2)
Refinement		
Resolution (Å)[¶]	20.32–2.71	38.58–2.19
No. reflections	42667	42704
R_{work}[‖]/R_{free}**	0.2161/0.2496	0.1753/0.2145
No. atoms		
Protein[††]	11485	5743
Ligand/ion	1	2
Water	190	224
B-factors		
Protein	55.54	35.16
Ligand/ion	79.98	60.20
Water	42.36	40.04
r.m.s. deviations		
Bond length (Å)[‡‡]	0.008	0.01
Bond angles (°)[‡‡]	0.94	1.06

*Statistics for highest resolution bin of reflections in parentheses.

[†]$R_{sym} = \Sigma_h \Sigma j\ 1\ I_{hj} - \langle I_h \rangle 1/\Sigma_h \Sigma_j I_{hj}$, where I_{hj} is the intensity of observation j of reflection h and $\langle I_h \rangle$ is the mean intensity for multiply recorded reflections.

[‡]Intensity signal-to-noise ratio.

[§]Completeness of the unique diffraction data.

[¶]Resolution cutoff used during heavy-atom refinement and phase calculations.

[‖]R-factor = $\Sigma_h\ |F_0| - |F_c|\ /\Sigma_h |F_0|$, where F_0 and F_c are the observed and calculated structure factor amplitudes for reflection h.

**R_{free} is calculated against a 10% random sampling of the reflections that were removed before structure refinement.

[††]Total number of protein atoms refined in the asymmetric unit.

[‡‡]Root mean square deviation of bond lengths and bond angles.